AIChE

Parametric Study and Estimation in CFD-Based PEM Fuel Cell Models

Parag Jain, Lorenz T. Biegler, and Myung S. Jhon
Dept. of Chemical Engineering, Carnegie Mellon University, Pittsburgh, PA 15213

DOI 10.1002/aic.11525
Published online June 18, 2008 in Wiley InterScience (www.interscience.wiley.com).

We propose an integrated modeling and optimization framework including detailed computational fluid dynamics based models and polymer electrolyte membrane fuel cell (PEMFC) systems. As an illustration, a multidimensional, multiphysics PEMFC model is constructed that accounts for major transport processes in the gas channels and the membrane electrode assembly. The resulting system of highly nonlinear partial differential-algebraic equations is fully discretized using a finite volume method, and the resulting large-scale nonlinear program is linked to a state-of-the-art interior point optimization algorithm. The framework is used for solving challenging parameter estimation problems resulting from incorporation of multiple experimental data points. Also, parametric studies are performed on detailed water transport mechanisms and distribution characteristics, and on overall system performance. Our proposed framework provides a robust and fast solution methodology, and is planned for modeling extensions and addressing other critical issues in PEMFC technology that require large-scale simulations. © 2008 American Institute of Chemical Engineers *AIChE J,* 54: 2089–2100, 2008
Keywords: fuel cells, optimization, simulation, process, PEM, integrated modeling, parameter estimation

Introduction

In the past two decades, research and development activities for commercialization of polymer electrolyte membrane (PEM) fuel cell (FC) systems have increased rapidly as a potential power source for portable electronic devices, automotive systems, and power plant applications. Compared with conventional battery systems, the advantages of these systems are high operating efficiency, near-zero greenhouse emissions, operation on renewable fuels, reliable operation, and nearly instantaneous rechargeable capabilities. Also, there is tremendous interest in the technology because of recent "quantum jumps" in the membrane electrode assembly (MEA), the region most critical to PEMFC performance.[1] In spite of these developments, several design and operation-related challenges need to be overcome before the commercial entry of PEMFCs. These issues can be addressed through an optimization problem with an objective of maximizing the power density and minimizing the cost, for a given durability. Solving this problem requires repeated experiments that may be expensive and time consuming as there are numerous degrees of freedoms in the system. With a plethora of parameters to be optimized and conditions to be satisfied, theoretical modeling is bound to play a pivotal role in achieving the objective.

Theoretical modeling in PEMFC systems is a complex task as the system is an integrated assembly of several interacting physical components, each comprising of multidimensional, multiphysical transport and/or reaction processes. There have been numerous PEMFC system modeling efforts beginning from the early 1990s.[2,3] The model in Springer et al.[2] assumed a perfectly mixed gas channel (GC), 1-D transport processes through gas diffusion layer (GDL), catalyst layer (CL) as a thin interface between GDL and PEM, and 1-D water transport within the PEM, thus accounting for nonuniform conductivity in the PEM. The model in Bernardi and Verbrugge,[3] incorporated a porous electrode model for the CL assuming, however, a fully hydrated PEM. Although, these models have limited applicability for large-scale FCs with high fuel utilization and wider operating ranges, they provided a fundamental basis for the forthcoming models. Gurau et al.[4] presented a 2-

Correspondence concerning this article should be addressed to L. T. Biegler at biegler@cmu.edu.

D transport model for a PEMFC and illustrated the utility of the model in examining multidimensional water and reactant distributions inside FC. Um et al.[5,6] applied computational fluid dynamics (CFD) approach to develop 2-D/3-D transport models. There have been numerous water management studies emphasizing on auto or low humidity operations.[7,8] In addition, various flow field patterns for bipolar plate design have been analyzed.[9] The state-of-the-art models are complex to the extent that they account for multidimensional mass, momenta, energy, species, and charge transport phenomena in different regions of a FC. Using available software architectures there have been attempts of hybrid 3-D dynamic modeling in PEMFC systems.[10] Modeling of GCs using Fluent^{TM} and MEA using gPROMS^{TM} softwares has been illustrated for a 3-D temperature analysis.[11] Other complex phenomena including two-phase flow with nonisothermal effects have received considerable attention as well.[12–17] However, many such transport and reaction processes in the system are not fully understood and are often modeled using semiempirical models containing unknown parameters. On the other hand, while more detailed and complex models claim to describe the physics more accurately, they generate more uncertain parameters. Hence, a rigorous methodology for parameter estimation for validating models with experimental data is a very useful tool for PEMFC systems. Moreover, an integrated systems model of PEMFC can be thought as a combination of interacting submodels of its various components. Hence, parameter estimation is especially attractive for two reasons: (i) From model reduction and simplification point of view, a particular subcomponent model may be modeled through a fitting function whereas more physics may be concentrated in other desired components and (ii) stand-alone measured properties of a subcomponent may differ when the component is integrated with the entire system under operation.

In spite of numerous modeling studies,[18] there have been only a few parameter estimation studies in PEMFCs. Suares and Hoo,[19] estimated model parameters based on the model by Nguyen and White,[20] who accounted for heat transfer between solid and liquid phases and latent heat associated with evaporation and condensation of water. The pseudo 2-D problem (1-D for GC, and 1-D PEM) was solved by discretizing the differential algebraic equation model using an orthogonal collocation method and by solving the associated nonlinear program (NLP) by the successive quadratic programming (SQP) approach. Applying a 1-D model, Berg et al.[21] fitted the voltage data for a specified current, from their experiments and estimated PEM conductivity, cathode exchange current density, PEM water transfer coefficient, and GDL oxygen mass transfer coefficient. Using 1-D charge and species balance in quiescent flow in GDL, CL, and PEM, Carnes and Djilali,[22] estimated PEM conductivity, GDL oxygen mass transfer coefficient, and exchange current densities by applying an algorithm for parameter estimation with partial differential equation (PDE) constraints based on a nonlinear least squares approach.

All the above parameter estimation studies, however, employ simpler PEMFC models with fewer individual component models, less detailed treatment of transport processes, and have been limited to 0- or 1-D. In particular, none of these studies have dealt with detailed water transport models in all the PEMFC components. These models are generally valid for a narrow range of operating conditions. As a result, the parameters obtained lead to uncertainty in model predictions for large FC applications, particularly with high fuel utilization and wide range of operation.

The reasons for these limitations in PEMFC parameter estimation studies are that the rigorous PEMFC models are multidimensional and possess multiphysical phenomena that involve a large coupled system of partial differential algebraic equations (PDAEs). These models have been generally solved using commercial CFD codes that are unequipped to deal with large-scale PDAE-constrained optimization problems associated with the corresponding parameter estimation problems.

In this article, we present an integrated modeling and optimization framework for multidimensional, multiphysical PEMFC models. We develop detailed transport models for GCs, GDLs, and PEM, along with a fitting function for the CL region, and formulate the parameter estimation problem as a PDAE-constrained optimization problem, with objective function that minimizes the model and experimental error between both input and output variables in the system. The problem is discretized in space leading to a large-scale NLP, which is solved using a robust and efficient state-of-the-art interior point optimization solver, IPOPT.[23] The problem is solved with multiple experimental data points, which cover a wide range of operating conditions, yielding parameters that lead to accurate model predictions. We further employ this framework to perform parametric studies on water transport mechanisms and distribution within the PEMFC system. We especially focus on parametric behavior of individual water transport processes within the PEM.

The remainder of the article is organized into the following components: physical modeling, parameter estimation, and parametric studies on water management in H_2 PEMFCs.

Physical Modeling of H_2 PEMFC

A schematic of a H_2 PEMFC and anode and cathode half cell reactions are shown in Figure 1. A H_2 PEMFC comprises of two GCs, two GDLs, and two CLs each on the anode and cathode sides, as well as a central PEM.

The GCs are bipolar plates that are hollow chambers for fluid inlet and outlet. They also serve as a connection between adjacent cells. The GDLs are porous materials (typically carbon paper or carbon cloth) which support the catalyst/support particles, provide uniform distribution of gases, and act as a medium for electron transport from the CL to the external current collectors. The CLs are the usually platinum (Pt) alloy particles supported on carbon, where the electrochemical reactions take place. PEM is generally polytetrafloroethylene chains with perflorosulfonate side groups. The PEM acts as a proton transport passage from anode to the cathode, and this conductivity of the PEM is a strong function of its water uptake. We will construct a 2-D macroscopic model illustrated in Figure 2. There are five chambers in the model, the GCs and the GDLs both on anode and the cathode sides, and a central PEM region. The humidified fuel and air are fed in the anode and cathode inlets, respectively. The species undergo a 2-D diffusion-convection process in both the GCs and the porous GDLs, after which they reach the PEM-GDL interface. On reaching the interface, hydrogen and oxygen undergo electrochemical reactions, and the water

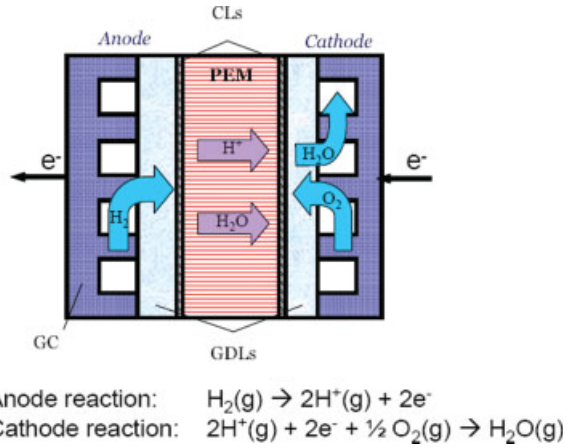

Figure 1. A schematic of the H_2 PEMFC, and the anode and cathode half cell reactions.

[Color figure can be viewed in the online issue, which is available at www.interscience.wiley.com.]

molecules are transported across the PEM from anode to the cathode. The protons released in the oxidation reaction at the anode are transported across the PEM, and electrons released reach the cathode via an external circuit. The protons and electrons on reaching the cathode combine with the oxygen in the reduction reaction to give water as the product.

The following assumptions are made in our model: (i) 2-D steady state model; (ii) isothermal condition is imposed in the entire modeling domain; (iii) both GDLs and PEM have isotropic porous media; (iv) the CLs are treated as thin interfaces between the GDLs and the PEM; (v) water remains in the vapor phase, and single phase flow takes place; (vi) cell current density remains constant; and (vii) anode overpotential is negligible in comparison with cathode overpotential and is neglected in the cell voltage calculation. In addition, the standard simplifications including laminar and incompressible flow, as well as negligible entrance effects have been imposed and numerically verified. In view of the assumptions made, we would stress here that the purpose of our work here is to build an integrated modeling and optimization framework for distributed CFD-based PEMFC models and the model presented here is for illustrative purposes. Hence, there are many significant physical features lacking in the model, such as the charge and energy balance equations, which are important in determining the potential, current density, and temperature distributions, and may have significant effect on cell performance at high current densities of operation. These will be added on to this framework in future.

The governing equations for each of the modeling regions, the interface and boundary conditions, and the empirical correlations adopted, are summarized in the list of Eqs. 1–19. A description of the variables can be found in the Notation section, whereas the model parameters and their values are listed in Table 1. The gas diffusion coefficients listed are computed via the Fuller-Schettler-Giddings equation for binary gas pairs (pg. 5–51 Ref. 24), where as the gas viscosities are computed using Wilke's expression.[25]

Equations 1 and 2 are continuity and isothermal Navier-Stokes (N-S) equations descriptive for the fluid flow within the GCs. The species mass transport (for H_2, H_2O, and O_2) is described by the diffusion-convection equation, Eq. 3. In modeling the GDL, the porosity (ε) of media is assumed to be constant, that is, there are no dilation and expansion effects. The total mass balance is described by Eq. 4. The N-S equation is modified by an additional Darcy's drag term ($\propto \mathbf{v}$) - Eq. 5.

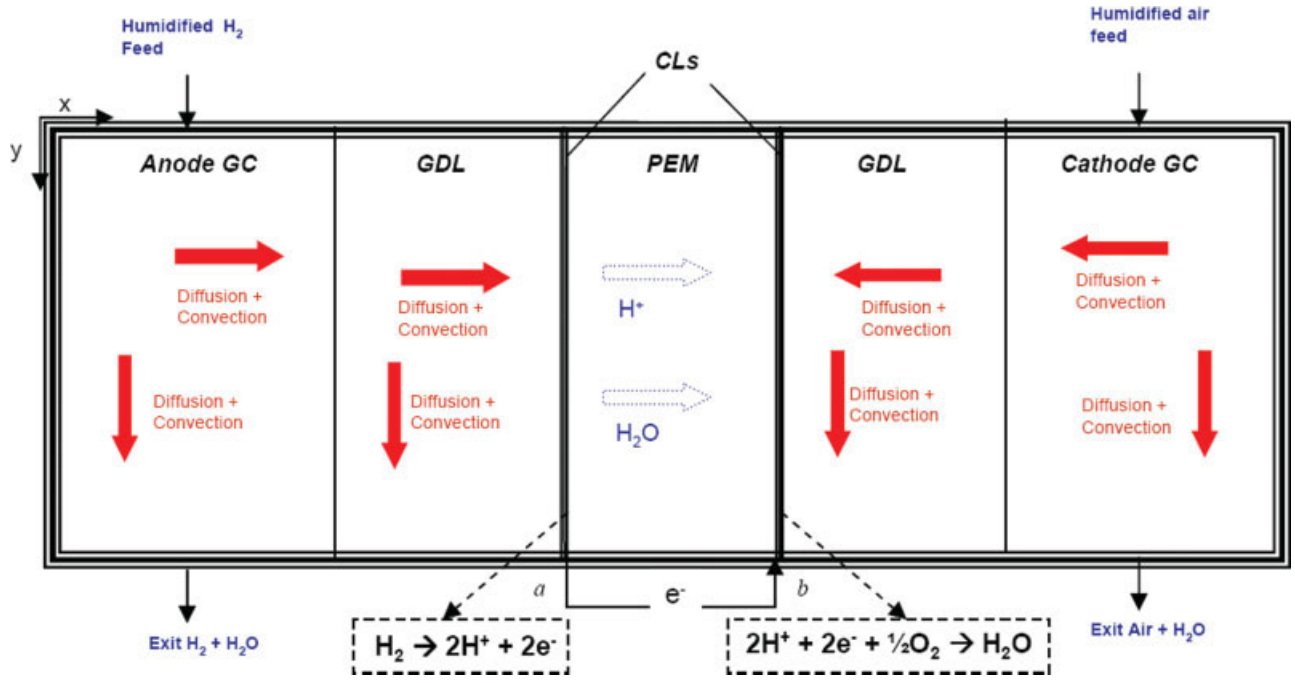

Figure 2. A schematic of the H_2 PEMFC model.

[Color figure can be viewed in the online issue, which is available at www.interscience.wiley.com.]

Table 1. Parameter Definitions and Values

Symbol	Description	Value
A_{ch}	Cell inlet area (m^2)	$L_{gc} \times$ width
A_m	Through plane direction area (m^2)	$L\times$ width
D_{H_2}	Hydrogen diffusion coefficient (m^2/s)	3.95×10^{-5}
$D_{H_2O,a}$	Anode water diffusion coefficient (m^2/s)	3.95×10^{-5}
$D_{H_2O,c}$	Cathode water diffusion coefficient (m^2/s)	6.8×10^{-6}
D_{O_2}	Oxygen diffusion coefficient (m^2/s)	5.6×10^{-6}
F	Faraday's constant (C/mol)	9.65×10^4
$\mathbf{i}$	Unit vector in x-direction	
k_m	PEM hydraulic permeability (m^2)	1.8×10^{-18}
K	GDL permeability (m^2)	1.76×10^{-11}
L	Length along GC (m)	7.36×10^{-2}
L_{gc}	GC width (m)	2.54×10^{-3}
L_{gd1}	GDL width (m)	2×10^{-4}
L_m	PEM thickness (m)	1.27×10^{-4}
M_{H_2}	Hydrogen molecular weight (kg/mol)	2×10^{-3}
M_{H_2O}	Water molecular weight (kg/mol)	1.8×10^{-2}
M_{O_2}	Oxygen molecular weight (kg/mol)	3.2×10^{-2}
M_m	PEM equivalent weight (kg/mol)	1.1
R	Gas constant (J/mol K)	8.314
T	Cell temperature (K)	353.15
ε	GDL porosity	0.4
ν_a^{eff}	Anode gas kinematic viscosity (m^2/s)	2.44×10^{-5}
ν_c^{eff}	Cathode gas kinematic viscosity (m^2/s)	4.1×10^{-6}
μ_m	PEM viscosity (kg/m s)	2.14×10^{-3}
ρ_a	Anode gas density (kg/m^3)	$C_{H_2,0}M_{H_2} + C_{H_2O,a}M_{H_2O}$
ρ_c	Cathode gas density (kg/m^3)	$C_{H_2,0}M_{H_2} + C_{H_2O,a}M_{H_2O} + C_{N_2,0}M_{N_2,0}$
ρ_m	PEM density (kg/m^3)	2×10^3
ξ_a	Anode stoichiometric coefficient	1.2
ξ_c	Cathode stoichiometric coefficient	2.6

GC equations

Total mass balance:

$$\nabla \cdot \mathbf{v} = 0 \tag{1}$$

Momentum balance:

$$\mathbf{M}(\mathbf{v}, p) \equiv \nabla \cdot (\mathbf{vv}) + \nabla \cdot (\upsilon^{\text{eff}} \nabla \mathbf{v}) + \frac{1}{\rho} \nabla p = 0 \tag{2}$$

Species mass balance:

$$S_i(C_i, D_i) \equiv \nabla \cdot (\mathbf{v} C_i) - \nabla \cdot (D_i \nabla C_i) = 0 \tag{3}$$

GDL equations

Total mass balance:

$$\nabla \cdot (\varepsilon \mathbf{v}) = 0 \tag{4}$$

Momentum balance:

$$\mathbf{M}(\varepsilon \mathbf{v}, \mathbf{p}) - \frac{\rho \nu^{\text{eff}}}{K} (\varepsilon^2 \mathbf{v}) = 0 \tag{5}$$

Species mass balance:

$$S_i(C_i, \varepsilon^{0.5} D_i) = 0 \tag{6}$$

Water transport in PEM

$$\left[1 - 8.8 \frac{F \rho_m k_m}{I M_m \mu_m} \frac{\partial p_w}{\partial x}\right] \frac{\partial \lambda}{\partial x} - 8.8 \frac{F D_{w,m} \rho_m}{I M_m} \left[\frac{\partial^2 \lambda}{\partial x^2} + \frac{\partial^2 \lambda}{\partial y^2}\right] = 0 \tag{7}$$

Boundary conditions

Interface conditions between PEM and GDL

H_2 consumption:

$$S_{H_2} = -\frac{M_{H_2}}{2F} I \tag{8}$$

H_2O transfer:

$$S_{H_2O} = -\alpha(x = a, y) \frac{M_{H_2O}}{2F} I \tag{9}$$

O_2 consumption:

$$S_{O_2} = -\frac{M_{O_2}}{4F} I \tag{10}$$

H_2O generation:

$$S_{H_2O} = (1 + \alpha(x = b, y)) \frac{M_{H_2O}}{2F} I \tag{11}$$

Inlet velocity conditions

At anode:

$$v_{0,a} = \xi_a \frac{A_m}{A_{ch}} \frac{I}{2F C_{H_2,0}} \tag{12}$$

At cathode:

$$v_{0,c} = \xi_c \frac{A_m}{A_{ch}} \frac{I}{4F C O_{2,0}} \tag{13}$$

Cell voltage equations

Output cell voltage:

$$V_{cell} = V_{OC} - \eta_c - \eta_{ohm} \tag{14}$$

Open circuit voltage:

$$V_{OC} = 1.23 - 0.9 \times 10^{-3}(T - 298.15) + \frac{RT}{4F} \ln(a_{H_2}^2 a_{O_2}) \tag{15}$$

Cathode overpotential:

$$\eta_c = \beta_1 \ln I + \beta_2 \tag{16}$$

Ohmic overpotential:

$$\eta_{ohm} = I \frac{L_m}{\sigma_{avg}} \tag{17}$$

Empirical correlations
PEM conductivity:

$$\sigma = (0.005139\lambda - 0.00326)\exp\left[\frac{1}{303} - \frac{1}{T}\right] \tag{18}$$

λ vs. vapor activity:

$$\lambda = \begin{cases} 0.04 + 17.81a_w - 39.85a_w^2 + 36a_w^2 & for\ 0 < a_w \leq 1 \\ 14 + 1.4(a_w - 1) & for\ 1 \leq a_w \leq 3 \end{cases} \tag{19}$$

The species mass transport equation, Eq. 6 is modified from the GC by multiplying D_i by a factor $\varepsilon^{0.5}$ to account for the porosity, as given by the Bruggman's relation.[5] Notice that $\varepsilon = 1$ recovers the GC species mass transport equation, Eq. 3.

The PEM is considered impermeable to all species except the protons and water. To describe the water transport in PEM, a quantity λ is introduced, which is the ratio of the water molecules to the number of sulphonate ion groups ($SO_3^- H^+$). It is related to PEM water concentration ($C_{w,m}$) by

$$\lambda = \frac{M_m C_{w,m}}{\rho_m} \tag{20}$$

The total flux ($\mathbf{N_{Tot}}$) of water in the PEM comprises of three parts: electro-osmotic drag ($\mathbf{N_{elec}}$), diffusion ($\mathbf{N_{diff}}$), and hydraulic permeation ($\mathbf{N_{hyd}}$).[26] The electro-osmotic drag originates from the flux due to drag on water molecules by proton molecules from anode to the cathode side. It is given by[2]:

$$\mathbf{N_{elec}} = \frac{2.5}{22}\frac{\lambda}{F}\mathbf{I} \tag{21}$$

The diffusion is caused by the concentration gradient because of nonuniform water distribution within the PEM, and is given by[2]:

$$\mathbf{N_{diff}} = \frac{D_{w,m}\rho_m}{M_m}\nabla\lambda \tag{22}$$

The hydraulic permeation is generated because of the pressure gradient between the anode and cathode sides. It is given by[26]:

$$\mathbf{N_{hyd}} = \frac{\rho_m k_m \lambda}{M_m \mu_m}\nabla p_w \tag{23}$$

After summing up these three flux terms, we imposed a differential water mass balance in the PEM. By assuming a steady state, we have

$$\nabla \cdot (\mathbf{N_{elec}} + \mathbf{N_{diff}} + \mathbf{N_{hyd}}) = 0 \tag{24}$$

which can be expressed as Eq. 7 in 2-D. Equations 8 and 10 represent the rate of consumption for H_2 and O_2 (mass per unit time) because of electrochemical reactions at anode and cathode CLs, respectively. In Eq. 9, S_{H_2O} is the mass transfer rate of H_2O across the PEM from anode to the cathode, and α is the moles of water molecules transported in x-direction from anode to the cathode side per mole of proton transported. It is given by the following equation,

$$\alpha = \frac{\mathbf{N_{Tot}} \cdot \mathbf{i}}{I/F} = 2.5\frac{\lambda}{22} - \frac{D_{w,m}\rho_m F}{M_m I}\frac{\partial\lambda}{\partial x} - \frac{\rho_m F k_m \lambda}{M_m I \mu_m}\frac{\partial p_w}{\partial x} \tag{25}$$

In Eq. 25, the three terms in the right hand side represent the electro-osmotic drag coefficient (ζ_{elec}), the back-diffusion coefficient (ζ_{diff}), and the hydraulic permeation coefficient (ζ_{hyd}), respectively. In Eq. 11, S_{H_2O} is the sum of the transfer rates of water molecules from anode to the cathode by electro-osmotic drag and water generation due to electrochemical reaction at cathode. Equations 12 and 13 represent the inlet velocity conditions at anode and cathode for specified stoichiometric ratios and current density.

The output cell voltage is calculated from Eq. 14. The open circuit cell voltage V_{OC} depends on the system temperature and pressure as shown in Eq. 15.[3] From Tafel kinetics, the cathode overpotential is modeled as a linear function of ln I with β_1 and β_2 as two fitting parameters (Eq. 16). The parameters β_1 and β_2 represent the electrode properties that influence the FC performance. The ohmic overpotential is given by Eq. 17. The PEM conductivity (σ) is correlated to water concentration (Eq. 18) as reported in Springer et al.[2] Finally, Eq. 19 provides relationship between λ and water vapor activity ($a_w = C_{H_2O}RT / P_{sat}$) at the GDL-PEM interface.[2]

The boundary conditions for the model are as follows: (i) at anode and cathode inlets, velocity and concentration values are specified; (ii) at anode and cathode exits, the flow is assumed to be fully developed and pressure is specified; (iii) at walls, no slip condition and zero normal species flux are employed; (iv) at GDL-PEM interface, no slip condition and interfacial species consumption Eqs. 8–11 are employed.

Parameter Estimation

Once the PEMFC model is constructed, we link the model to IPOPT, and perform parameter estimation. Here we first present the parameter estimation problem formulation, followed by the details of numerical procedure, and application to PEMFC system.

Problem formulation

The model Eqs. 1–19 form a set of PDAEs which is cast in the following compact form:

$$\begin{aligned} &\mathbf{g}\left[\frac{\partial \mathbf{z}}{\partial x}, \frac{\partial \mathbf{z}}{\partial y}, \frac{\partial^2 \mathbf{z}}{\partial x^2}, \frac{\partial^2 \mathbf{z}}{\partial y^2}, \mathbf{z}(X), \mathbf{w}(X), X, \mathbf{p}\right] = 0 \\ &\mathbf{h}[\mathbf{z}(X), \mathbf{w}(X), X, \mathbf{p}] = 0 \\ &\mathbf{B}[\mathbf{z}(0), \mathbf{z}(1), \dot{\mathbf{z}}(0), \dot{\mathbf{z}}(1)] = 0 \end{aligned} \tag{26}$$

Here, $\mathbf{z}$ denotes the differential state variables. The symbol $\mathbf{w}$ represents the algebraic variables, and $\mathbf{p}$, the parameters. The symbol X represents the set $\{x, y\}$ of independent variables. The PDEs comprising of momentum, species mass, and total mass balance equations are denoted by $\mathbf{g}[\cdot]$, the algebraic equations including the cell voltage calculation equations and empirical correlations by $\mathbf{h}[\cdot]$, and the boundary conditions by $\mathbf{B}[\cdot]$. In (26), the bold symbol represents a vector.

For parameter estimation problem formulation, an appropriate objective function needs to be chosen. Standard least-squares formulation approach leads to parameter estimates that minimize the error between model and experimental output variables, and therefore account only for errors due to model inadequacy and random errors in measurement of output variables. If the input variables have measurement errors as well, this approach however, is well known to give biased parameters.[27] For this, we employ the errors-in-variables-measured (EVM) formulation approach, that takes into account the errors of all measured variables, both inputs and outputs to the system. The corresponding parameter estimation problem is formulated as the following optimization problem:

$$\begin{aligned}
&\min_{\mathbf{p}} \sum_{i=1}^{N} \Big[(\mathbf{w}_{i,\mathrm{o}} - \mathbf{w}_{i,\mathrm{o}}^{M})^{T} \mathbf{V}_{\mathbf{w},\mathrm{o}}^{-1} (\mathbf{w}_{i,\mathrm{o}} - \mathbf{w}_{i,\mathrm{o}}^{M}) \\
&\qquad + (\mathbf{w}_{i,\mathrm{I}} - \mathbf{w}_{i,\mathrm{I}}^{M})^{T} \mathbf{V}_{\mathbf{w},\mathrm{I}}^{-1} (\mathbf{w}_{i,\mathrm{I}} - \mathbf{w}_{i,\mathrm{I}}^{M}) \Big] \\
&\text{s.t. } \mathbf{g}_i \left[\frac{\partial \mathbf{z}_i}{\partial x}, \frac{\partial \mathbf{z}_i}{\partial y}, \frac{\partial^2 \mathbf{z}_i}{\partial x^2}, \frac{\partial^2 \mathbf{z}_i}{\partial y^2}, \mathbf{z}_i(X), \mathbf{w}(X), X, \mathbf{p} \right] = 0 \\
&\mathbf{h}_i[\mathbf{z}_i(X), \mathbf{w}_i(X), X, \mathbf{p}] = 0 \\
&\mathbf{B}_i[\mathbf{z}_i(0), \mathbf{z}_i(1), \dot{\mathbf{z}}_i(0), \dot{\mathbf{z}}_i(1)] = 0 \\
&i \in \{1, 2, \ldots, N\}
\end{aligned} \tag{27}$$

where, N is the number of experimental data sets and index i is used to replicate the model equations and variables for each of these data sets. The first summation term in the objective represents the least squares error between the model and experimental output variables, $\mathbf{w}_{i,\mathrm{O}}$ and $\mathbf{w}_{i,\mathrm{O}}^{M}$ respectively, whereas the second term represents the error between the input variables $\mathbf{w}_{i,I}$ and $\mathbf{w}_{i,I}^{M}$ · $\mathbf{V}_{\mathrm{w,O}}^{-1}$ and $\mathbf{V}_{\mathrm{w,I}}^{-1}$ denote the weighting matrices for output and input variables, respectively, and represent the inverse of the corresponding covariance matrices. Superscript T represents the matrix transpose operator. The EVM formulation, however, leads to an increase in the number of degrees of freedom in the optimization problem (27) by the number of data sets used in the problem, often posing additional computational challenges in optimization. The EVM variables are the current density, I (input), and cell voltage, V (output) in this study.

Numerical procedure

The transport equations within the GC, GDL, and PEM compartments are discretized using a finite volume method (FVM). The entire modeling domain was subdivided into finite volumes. We employed the staggered grid approach, where the velocity field components are defined at a staggered location on the grid with respect to the concentration and pressure variables. We have adopted the discretization procedure given in Patankar.[28]

Discretized equations of the PDAE system can be formulated as a generalized NLP of the following form,

$$\begin{aligned}
&\min f(x) \\
&s.t\ c(x) = 0 \\
&x_{\mathrm{L}} \le x \le x_{\mathrm{U}}
\end{aligned} \tag{28}$$

The NLP algorithm employed in our study is IPOPT.[23] This algorithm is based on a barrier approach in which the variable bounds are treated by adding a logarithmic barrier term to the objective function, which casts the problem in (28) into the following form,

$$\begin{aligned}
&\min \varphi(x) = f(x) - \hat{\mu} \sum_{i=1}^{N} \ln(x^{(i)} - x_{\mathrm{L}}^{(i)}) - \hat{\mu} \sum_{i=1}^{N} \ln(x^{(i)} - x_{\mathrm{U}}^{(i)}) \\
&\text{s.t } c(x) = 0
\end{aligned} \tag{29}$$

with a barrier parameter $\hat{\mu} > 0$. Here, $x^{(i)}$ denotes the ith component of the vector x. The degree of influence of the barrier is determined by the size of $\hat{\mu}$, and under mild conditions $x_*(\hat{\mu})$ converges to a local solution x_* of the original problem (28) as $\hat{\mu} \to 0$.[29] Consequently, a strategy for solving the original NLP is to solve a sequence of barrier problems (29) for decreasing barrier parameters $\hat{\mu}_l$, where l is the counter for the sequence of subproblems.

IPOPT follows a primal-dual approach and applies a Newton's method to the optimality conditions of (29), leading to solution of the following linear system at each iteration k:

$$\begin{bmatrix} H_{\mathrm{k}} + \sum_{\mathrm{k}} & A_{\mathrm{k}}^{T} \\ A_{\mathrm{k}} & 0 \end{bmatrix} \begin{bmatrix} \Delta x \\ \Delta \Lambda \end{bmatrix} = - \begin{bmatrix} \nabla \varphi(x_{\mathrm{k}}) + \nabla c(x_{\mathrm{k}})^{T} \Lambda_{\mathrm{k}} \\ c(x_{\mathrm{k}}) \end{bmatrix} \tag{30}$$

where we use the convention, $X = \mathrm{diag}(x)$, etc., H_{k} is the Hessian of the Lagrangian function $f(x_{\mathrm{k}}) + c(x_{\mathrm{k}})^{T}\ \Lambda_{\mathrm{k}}$, $A_{\mathrm{k}} = \nabla c(x_{\mathrm{k}})$, and $\Sigma_{\mathrm{k}} = (X_{\mathrm{k}} - X_{\mathrm{L}})^{-1}\ (V_a^{\mathrm{k}}) + (X_{\mathrm{U}} - X_{\mathrm{k}})^{-1}\ (V_b^{\mathrm{k}})$ is the barrier term. Global convergence of the Newton's method is promoted by a novel filter line search strategy; detailed analysis shows both global convergence and fast local convergence properties. More information on IPOPT can be found in Wächter and Biegler,[23] and on the following website: https://projects.coin-or.org/Ipopt.

The discretization of the NLP using FVM was performed manually for all the equations and physical modeling domains. This CFD implementation was carefully verified with the commercial CFD softwares (Fluent$^{\mathrm{TM}}$ and FEMLAB$^{\mathrm{TM}}$); however, no automated CFD software was employed to build this model. Instead for all calculations the discretized equations were programmed in the modeling environment AMPL,[30] which was linked to the IPOPT solver.

Application to PEMFC system

We now illustrate the above methodology for parameter estimation in PEMFC models using the current–voltage (I–V) data from Ticianelli et al.[31] (from Figure 5, 20 wt % Pt/C in supported electrocatalyst plus 50 *nm* sputtered film of Pt, 0.45 mg/cm^2 of Pt. T = 353 k, p = 3/5 atm), with output variable as V, and input variable as I. The goal here is to find parameter plus model combination which validates the experimental data for a wide range of operating conditions, which is achieved by using multiple I–V data points in the parameter estimation problem. The model equations are replicated depending on the number of I–V points chosen. The EVM approach minimizes the orthogonal distance between model and experimental points on the global I–V curve.

Model Parameters. We choose to estimate the following parameters in the PEMFC system:

PEM water diffusion coefficient. The significance in estimating this property lies in the accurate prediction of water holdup and transport characteristics within the PEM, which in turn is critical to the water management issue. However, the PEM diffusion coefficient depends on the PEM structure, the

Table 2. Parameter Estimates for Different Number of *I−V* Data Point Cases

I - *V* Points	$10^9 D_{w,m}(m^2/S)$	β_1	β_2
3	1.77	0.054	0.423
4	1.64	0.047	0.416
7	1.60	0.045	0.412
11	1.72	0.047	0.418

pretreatment method used for a PEM type, its water uptake, and the counter-ions in the system, thus increasing the number of cases for which experiments need to be performed.[32] The experimental studies performed[2,33] have been limited mainly to Nafion™ stand-alone PEMs, and there is scarcity of data for other PEMs, especially with in situ measurements. Our work, for the first time provides a systematic framework for estimating diffusion coefficients using a multidimensional, multiphysics modeling and optimization framework.

Parameters β_1 and β_2 in CL. The focus of current study is water management and hence detailed physics is incorporated within the PEM. Within the CL region, we employ a Tafel type equation for cathode overpotential (Eq. 16), with β_1 and β_2 representing the electrode properties.

Results

The EVM problem was solved for 3, 4, 7, and 11 *I–V* data points and the estimated parameter values are summarized in Table 2.

The values of $D_{w,m}$ are within the range of values reported by other semiempirical and experimental data sources.[33,34] On comparison of Eq. 16 with Tafel overpotential expression,[35] the values of β_1 and β_2 from the 11-point case correspond to an electrode charge transfer coefficient value of 0.32 and a exchange current density value of 1.37×10^{-4} A/cm^2 which are well within their respective physical ranges. The fitted *I–V* curve for the 11-point case is illustrated in Figure 3.

Table 3 illustrates the computational details of the associated NLPs for different data point cases. NZJ and NZH denote the number of nonzero entries in the Jacobian and Hessian matrices, respectively.

The problems were solved on a 3.4 GHz processor, 4 Gb RAM, Pentium IV machine. The problems in each case were initialized by the solution of square problem simulation cases. The value of the objective (residual) for the 3-point case, which corresponds to same number of parameters as the number of data points, comes out to be nearly zero. Also the residual values increase with number of data points, as expected. The CPU times scale linearly with problem size. The 11-point case corresponds to a large-scale NLP of 73, 120 variables which is solved in little over 4 min. Hence, the current optimization framework seems to be reliable and computationally efficient in dealing with larger parameter estimation and optimization problems in PEMFC systems.

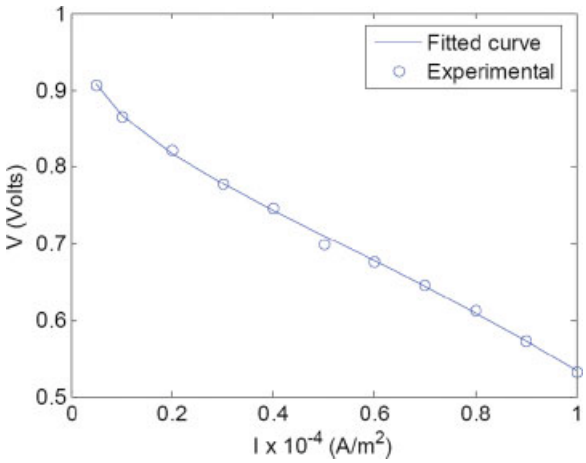

Figure 3. The fitted *I–V* curve for the 11-point case.

[Color figure can be viewed in the online issue, which is available at www.interscience.wiley.com.]

Moreover, the reduced Hessian matrix at the solution of each of the problems is positive definite, which corresponds to the fact that the parameters estimated are unique.

Parametric Studies

In this section, we present parametric study results which focus on the water management issue in PEMFCs. Water management refers to the act of ensuring sufficient hydration of PEM to avoid ohmic losses and to avoid liquid water flooding (thus, ensuring efficient product water removal) that blocks the active CL sites and GDL pores, thus hindering the gas transport from the GC inlet to the CL. The problem boils down to designing the GDL (porosity and hydrophobicity), the CL (thickness, composition, and particle size distribution), and determining optimal operating and design conditions (e.g., optimal flow characteristics, inlet humidity, geometric parameters, temperature, pressure, and current density), that achieve the above goal.

Numerous water management studies in the PEMFC literature elucidate water transport characteristics with various design and operating parameters in the system.[18] Hence the goal of current work is twofold: to validate our modeling and optimization framework by reproducing similar parametric behaviors as reported in previous studies and then, to examine in more detail the parametric behavior of individual water transport processes especially within the PEM. In this section, using the parameters estimated from previous section, we perform parametric studies to see the effect of flow arrangement (co-flow or counter-flow with respect to anode and cathode inlet locations), inlet gas humidity, and PEM thickness on water transport mechanisms and distribution in the system, and overall cell performance.

Table 3. Computational Details for Each of Multiple Data Point Cases

I - *V* Points	Residual	Variables	Constraints	Iterations	CPUs	NZJ	NZH
3	6.97×10^{-13}	19,944	19,938	17	49.06	115,815	34,599
4	3.58×10^{-05}	26,591	26,584	17	55.59	154,420	46,132
7	6.27×10^{-05}	46,532	46,522	25	143.19	270,235	80,731
11	3.48×10^{-04}	73,120	73,106	23	259.54	424,655	126,863

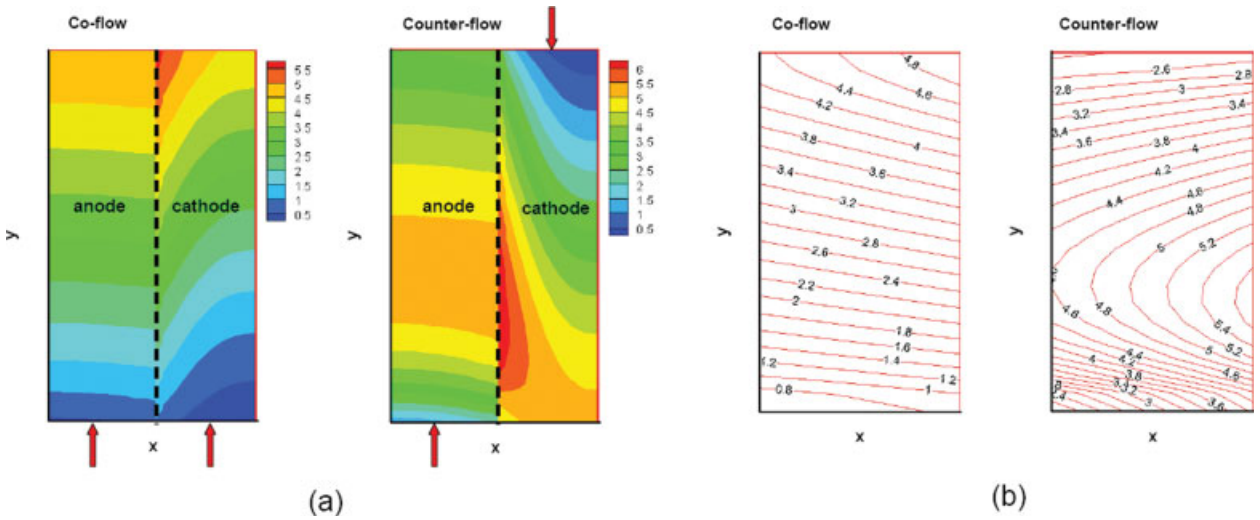

Figure 4. Water concentration (mol/m^3) profiles in (a) anode and cathode regions and (b) PEM water profiles (λ), for co-flow (Left) and counter-flow (Right) cases.

[Color figure can be viewed in the online issue, which is available at www.interscience.wiley.com.]

Flow arrangement

We first examine the effect of changing inlet gas flow directions in anode and cathode GCs on the cell water distribution and on overall performance. As observed from Figure 4a (Left), in the co-flow arrangement, water concentration increases monotonically from the inlet to the outlet of the GCs, both within the anode and the cathode regions. Also, the PEM water concentration [Figure 4b (Left)] follows a monotonically decreasing trend from cathode to the anode side. On the other hand, in the counter-flow arrangement (Right sides of Figures 4a, b), there exists a maxima of water concentration in the middle region in both anode and cathode sides, and in the PEM region. Also, the gradient of water concentration in the PEM becomes multidirectional.

More detailed water transport characteristics can be observed from Figures 5a, b, which show the variation of individual water transport coefficients, defined earlier in Eq. 25, along the anode GDL-PEM interface for the co-flow and the counter-flow arrangements. For the co-flow arrangement (Figure 5a), the electro-osmotic drag effect, which is directly proportional to λ, increases monotonically, but the diffusion effect acting in the opposite direction also increases at a similar rate. Since the anode and cathode pressures have been taken equal in these parametric studies, ζ_{hyd} remains zero throughout the length along the interface. The overall water transport coefficient α is therefore simply a summation of ζ_{elec} and ζ_{diff}, and remains constant and negative, as the diffusion effect dominates over the electro-osmotic drag effect.

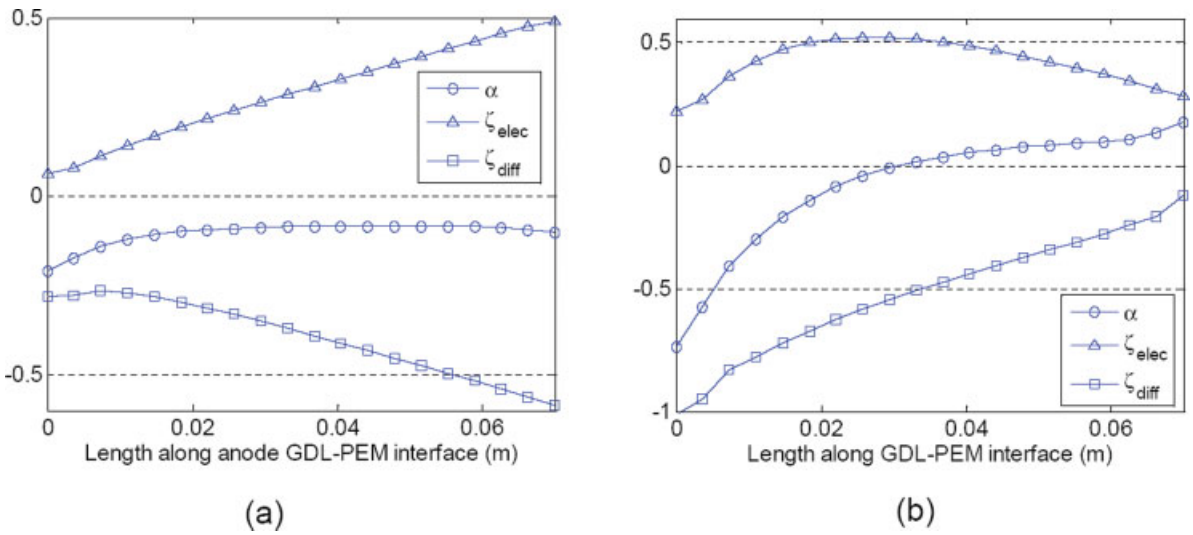

Figure 5. Variation of PEM water transport coefficients along the anode GDL-PEM interface for (a) co-flow and (b) counter-flow cases.

[Color figure can be viewed in the online issue, which is available at www.interscience.wiley.com.]

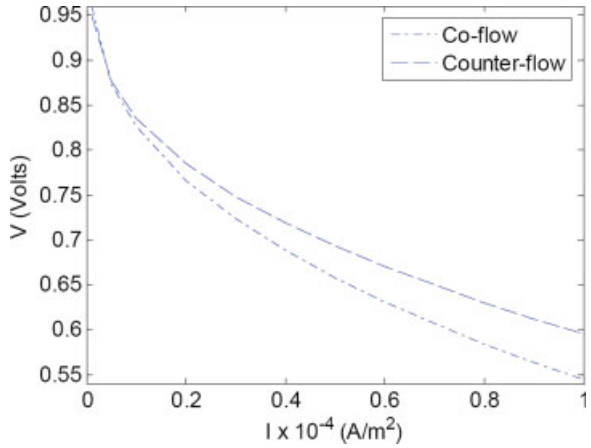

Figure 6. Polarization curves for counter-flow and co-flow cases.

[Color figure can be viewed in the online issue, which is available at www.interscience.wiley.com.]

For the counter-flow case (Figure 5b), however, electro-osmotic drag coefficient possesses a maximum because of a maximum in water concentration along the GDL-PEM interface, whereas the back-diffusion coefficient increases sharply. The sign of α changes along the interface from negative to positive, which indicates the presence of an internal water recirculation in the counter-flow arrangement. This recirculation mechanism causes the PEM to hold higher amount of water and therefore, leads to a better performance via enhanced conductivity. The improved performance of the counter-flow case can be seen in Figure 6 which compares the *I–V* characteristic curves for the two flow arrangements. The disparity in the performances is especially visible for dry to low humidities, and for lower pressures of operation. However, for higher humidification conditions, the flow arrangement does not seem to affect the cell performance.

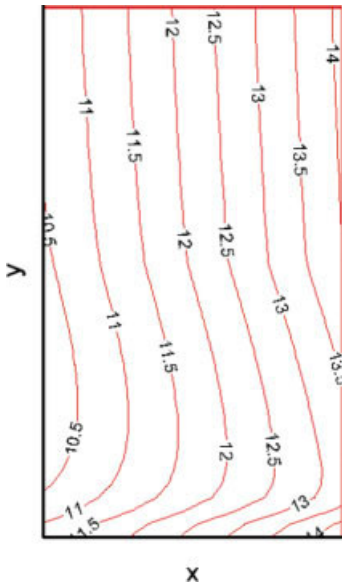

Figure 7. PEM water concentration profile for RH = 80/80.

[Color figure can be viewed in the online issue, which is available at www.interscience.wiley.com.]

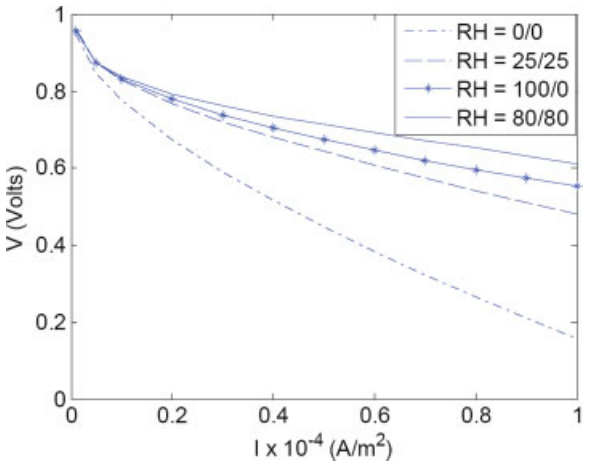

Figure 8. Polarization curves for different inlet humidity cases.

[Color figure can be viewed in the online issue, which is available at www.interscience.wiley.com.]

Inlet humidity

As inlet gas humidities increase, the overall water uptake in the system increases, which increases the ionic conductivity of the PEM and enhances the overall system performance. Figures 4b, Left and 7 compare the PEM water uptake of a totally dry inlet gas stream and the case where inlet humidities are set equal to 80/80 (xx/xx denotes relative humidity (RH) values at the anode and the cathode sides, respectively) in a co-flow arrangement. The average PEM water uptake increases by approximately four times in the latter case.

As seen from Figure 8, the cell performance improves significantly from dry conditions to low humidity conditions (25 % RH in each anode and cathode side), and the performance further improves in the cases of inlet humidities set equal to 100/0 and 80/80.

Figures 9a, b display the α and ζ_{elec} curves for a co-flow arrangement with inlet humidities set as 80/80. In contrast to totally dry inlet humidity case where there is a unidirectional water flux from cathode to the anode side, the water transport in high inlet humidity case takes place from anode to the cathode side until a certain distance along the length, after which the water transport direction reverses, as indicated by the switching in the sign of α in between. This may be explained in the following manner: for higher inlet humidity case, due to high water concentration near inlet, the electro-osmotic drag effect dominates over the diffusion effect and there is net transport of water from anode to the cathode side. However, further down the channel, because of this loss of water from anode, and because of water production in the electrochemical reaction at the cathode, a sufficiently high water concentration gradient sets up in the opposite direction, and diffusion effect dominates over the electro-osmotic drag effect.

PEM thickness

PEM thickness affects the PEM conductivity in two main ways: (i) through an increase or decrease in the proton transport path and (ii) through water distribution characteristics.

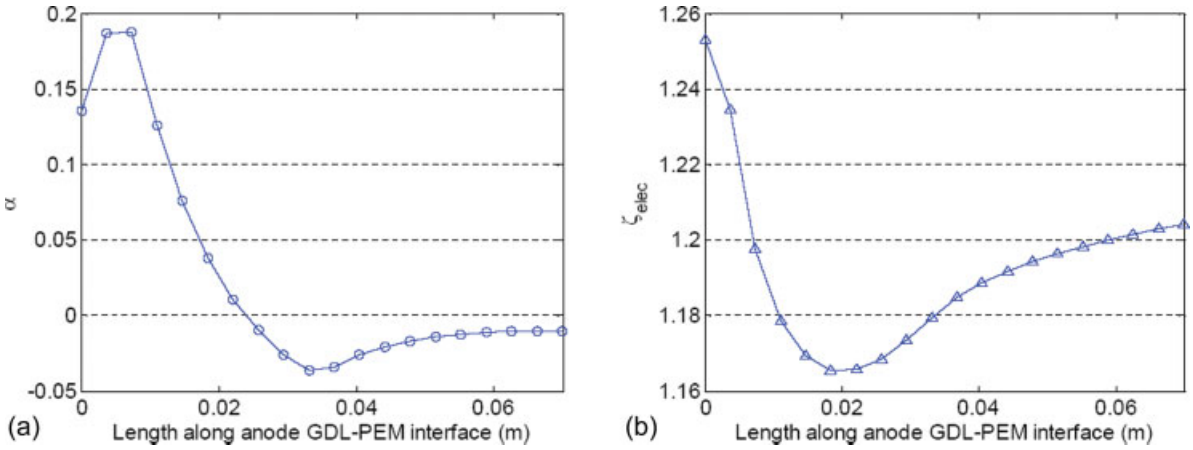

Figure 9. Variation of α and ζ_{elec} along the anode GDL-PEM interface for RH = 80/80.

[Color figure can be viewed in the online issue, which is available at www.interscience.wiley.com.]

Figures 10a, b compare the water transport coefficients of Nafion^{TM} 117 (thickness 178 μm) and Nafion^{TM} 111 (thickness 25.4 μm) PEMs.

Although there is only a slight modification in the overall transport coefficient α which becomes more negative for Nafion^{TM} 111, ζ_{elec} and ζ_{diff} increase significantly in magnitude, indicating increased water transport in Nafion^{TM} 111 as compared with Nafion^{TM} 117 in either the right or the left directions. This causes the water concentration to be more uniform in the x-direction for a thinner PEM as compared with a thicker PEM (Figures 11a, b).

Hence, there exist regions (for high y values), within thinner PEMs where water concentration is uniformly high along the entire x-direction (or PEM width), which provide least resistance paths for proton transport. On the other hand, for thicker PEMs, water distribution is such that there are fewer, or no such regions of high proton conductivity along the entire PEM width. Figure 12 shows a large difference in performances of Nafion^{TM} 117 and Nafion^{TM} 111 PEMFCs. However, as shown in Figure 12, counter-flow arrangement still leads to a better performance than the co-flow arrangement due to increased PEM conductivity via internal water recirculation.

Conclusions

In this article, we propose a generalized modeling and optimization framework for rigorous CFD models in PEMFC systems. We develop a comprehensive multidimensional PEMFC model that takes into account major transport processes in the GCs and the MEA. A detailed water transport equation, accounting for electro-osmotic drag, diffusion, and hydraulic permeation, is also incorporated into the model assuming single-phase flows. The resulting system of PDAEs is fully discretized using a finite volume scheme leading to a large-scale nonlinear system of equations which is linked to IPOPT solver.

Using this framework parameter estimation is performed to estimate CL fitting parameters and PEM water diffusion coefficient, thus illustrating the utility of parameter estimation as a tool complementary to modeling, for the regions where system is modeled with a lumped parameter approach. We employed

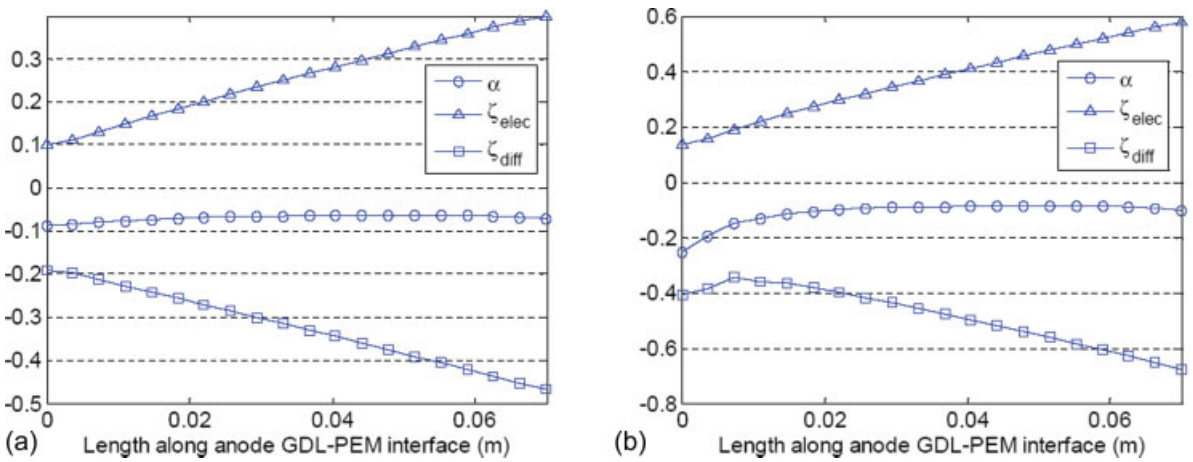

Figure 10. Variation of PEM water transport coefficients along the anode GDL-PEM interface for: (a) Nafion^{TM} 117 and (b) Nafion^{TM} 111 PEMs.

[Color figure can be viewed in the online issue, which is available at www.interscience.wiley.com.]

EVM formulation to multiple *I–V* data point cases that yield parameter estimates such that model predictions are accurate for wide operation ranges. The proposed methodology leads to fast and efficient solution of large-scale NLPs in a few CPU seconds and a few iterations. The parameters from different data point cases are determined uniquely.

We further employ this framework to perform water management parametric studies to examine water transport mechanisms and distribution, especially within the PEM, and to examine the overall system performance. The conclusions made here are based on the assumptions of single phase, isothermal system which will be relaxed in our future work. However, the operating conditions in the simulations here are chosen to ensure that the partial pressure of water remains below its saturation pressure. We observe that counter-flow arrangement leads to better performance than the co-flow arrangement especially for the conditions of low inlet humidity and low pressure, due to an internal water recirculation mechanism which facilitates higher PEM hydration. Moreover, as inlet gas humidities increase the overall water uptake in the system increases which improves the ionic conductivity of the PEM and enhances the overall system performance. Also, thin PEMs perform significantly better than thicker PEMs due to their smaller resistance path to proton transport, and due to a more uniform water distribution along the x-direction.

Finally, the methodology presented in this article can be adapted to incorporate additional physics not considered here. Charge and energy transport equations can be handled in a numerically similar manner to the momenta and species transport equations. However, these additions may introduce more nonconvexities and that the reduced Hessian matrix may not be positive definite everywhere. The IPOPT solver has an important feature in assessing second derivative properties; through the inertia of the Karush-Kuhn-Tucker matrix,[23] IPOPT monitors and corrects the eigen-structure of the reduced Hessian matrix if it is not positive definite, thus ensuring descent properties, and it verifies whether the parameters are unique by reporting the state of the reduced Hessian at the optimum. Also, the generalization to 3-D transport phenomena can be included through the IPOPT solver. The object oriented form of IPOPT is ideal for large-scale PDAE constrained optimization problems, as it can be adapted to this structure. This has already been tested successfully for 3-D problems with considerably larger number of equations/variables than considered in this study.[36]

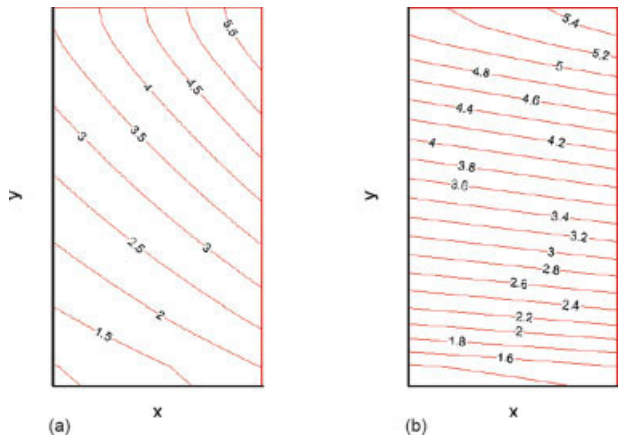

Figure 11. PEM water concentration profiles for: (a) co-flow and (b) counter-flow cases.

[Color figure can be viewed in the online issue, which is available at www.interscience.wiley.com.]

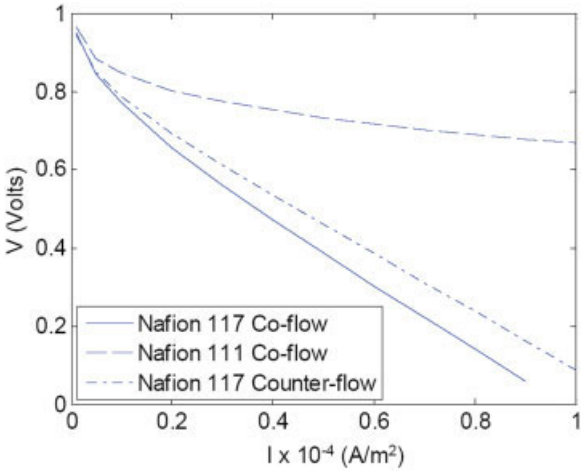

Figure 12. *I–V* characteristic curves for Nafion™ 117 and Nafion™ 111 PEMFCs.

[Color figure can be viewed in the online issue, which is available at www.interscience.wiley.com.]

Acknowledgments

Funding from the National Science Foundation (Grant CTS-0438279) and the Pennsylvania Infrastructure Technology Alliance is gratefully acknowledged. The authors also are grateful to Dr. S. Ou and Prof. L.E.K. Achenie for useful discussions and assistance on model development.

Notation

a = activity
A = area, m^2
$\mathbf{B}[\cdot]$ = vector of boundary conditions
C = molar concentration, mol/m^3
diag = diagonal matrix operator
D_i = diffusion coefficient for species i, m^2/s
F = Faraday's constant, C/mol
$\mathbf{g}[\cdot]$ = vector of PDEs
$\mathbf{h}[\cdot]$ = vector of algebraic equations
H_k = Hessian of the Lagrangian function
$\mathbf{i}$ = unit vector in x-direction
I = current density, A/m^2
$\mathbf{I}$ = current density vector, A/m^2
k = hydraulic permeability, m^2
K = GDL permeability, m^2
L = length, m
M_i = molecular weight of species i, kg/mol
N = number of data sets
$\mathbf{N}$ = flux, mol/m^2 s
p = pressure, N/m^2
$\mathbf{p}$ = vector of parameters
R = gas constant, J/mol K
S = consumption/production rate, kg/s
T = temperature, K
v_0 = inlet velocity, m/s
$\mathbf{v}$ = velocity vector, m/s
V = voltage, Volt
$\mathbf{V}$ = covariance matrix
$\mathbf{w}$ = vector of algebraic variables
X = set of independent variables

$\mathbf{z}$ = vector of differential variables
$\dot{\mathbf{z}}$ = vector of derivative of differential variables

Greek letters

α = $[H_2O]/[H^+]$ transported
$\beta_i (i = 1,2)$ = catalyst layer fitting parameters, Volt
ε = GDL porosity
η = overpotential loss, Volt
ζ = PEM water transport coefficient, dimensionless
λ = $[H_2O]/[H^+]$ in PEM
Λ = Lagrange multiplier
μ = viscosity, kg/m s
$\hat{\mu}$ = barrier parameter
ν = kinematic viscosity, m^2/s
ρ = density, kg/m^3
σ = PEM conductivity, $S\text{-}m^{-1}$
Σ_k = barrier term
ξ = stoichiometric ratio

Subscripts and superscripts

a = anode
avg = average
c = cathode
ch = channel
diff = diffusion
eff = effective value
elec = electro-osmotic drag
gc = gas channel
gdl = gas diffusion layer
hyd = hydraulic permeation
I = input
L = lower bound
m = PEM
M = measured
O = output
OC = open circuit
ohm = ohmic
sat = saturation value
T = matrix transpose operator
Tot = total
U = upper bound
w = water
0 = value at initial conditions

Literature Cited

1. Costamagna P, Srinivasan S. Quantum jumps in the PEMFC science and technology from the 1960s to the year 2000: Part I. Fundamental scientific aspects. *J Power Sources*. 2001;102:242–252.
2. Springer TE, Zawodzinski TA, Gottesfeld S. Polymer electrolyte membrane fuel cell model. *J Electrochem Soc*. 1991;136:2334–2342.
3. Bernardi DM, Verbrugge MW. Mathematical model of a gas diffusion electrode bonded to a polymer electrode. *AIChE J*. 1991;37:1151–1163.
4. Gurau V, Liu H, Kakac S. Two-dimensional model for proton exchange membrane fuel cells. *AIChE J*. 1998;44:2410–2422.
5. Um S, Wang CY, Chen KS. Computational fluid dynamics modeling of proton exchange membrane fuel cells. *J Electrochem Soc*. 2000; 147:4485–4493.
6. Um S, Wang CY. Three-dimensional analysis of transport and electrochemical reactions in polymer electrolyte fuel cells. *J Power Sources*. 2004;125:40–51.
7. Hogarth WHJ, Benziger JB. Operation of polymer electrolyte membrane fuel cells with dry feeds: design and operating strategies. *J Power Sources*. 2006;159:968–978.
8. Um S, Wang CY. Computational study of water transport in proton exchange membrane fuel cells. *J Power Sources*. 2006;156:211–223.
9. Hyun M, Kim S, Jung D, Lee B, Peck D, Kim T, Shul Y. Prediction of anode performances of direct methanol fuel cells with different flow-field design using computational simulation. *J Power Sources*. 2006;157:875–885.
10. Pantelides CC. Process modeling technology: A critical review of recent developments. *Proceedings of the FOCAPD*. Princeton, NJ: 2004;69–82.
11. Matzopoulos M. Advanced modeling accelerates fuel cell development. *FC Focus*. September, 2007;44–47.
12. He W, Yi JS, Nguyen TV. Two-phase flow model of the cathode of PEM fuel cells using interdigitated flow fields. *AIChE J*. 2004;46: 2053–2064.
13. Wang ZH, Wang CY, Chen KS. Two-phase flow and transport in the air cathode of proton exchange membrane fuel cells. *J Power Sources*. 2001;94:40–50.
14. You L, Liu H. A two-phase flow and transport model for the cathode of PEM fuel cells. *Int J Heat Mass Transfer*. 2002;45:2277–2287.
15. Nam H, Kaviany M. Effective diffusivity and water-saturation distribution in single- and two-layer PEMFC diffusion medium. *Int J Heat Mass Transfer*. 2003;46:4595–4611.
16. Ju H, Meng H, Wang CY. A single-phase, non-isothermal model for PEM fuel cells. *Int J Heat Mass Transfer*. 2005;48:1303–1315.
17. Wang Y, Wang CY. A Nonisothermal, two-phase model for polymer electrolyte fuel cells. *J Electrochem Soc*. 2006;153:A1193–A1200.
18. Wang CY. Fundamental models for fuel cell engineering. *Chem Rev*. 2004;104:4727–4766.
19. Suares GE, Hoo KA. Parameter estimation of a proton-exchange membrane fuel cell using voltage-current data. *Chem Eng Sci*. 2000;55:2237–2247.
20. Nguyen TV, White RE. A water and heat management model for proton-exchange-membrane fuel cells. *J Electrochem Soc*. 1993;140: 2178–2186.
21. Berg P, Promislow K, Pierre JS, Stumper J. Water management in PEM fuel cells. *J Electrochem Soc*. 2004;151:A341–A353.
22. Carnes B, Djilali N. Systematic parameter estimation for PEM fuel cell models. *J Power Sources*. 2005;144:83–93.
23. Wächter A, Biegler LT. On the implementation of an interior-point filter line-search algorithm for large-scale nonlinear programming. *Math Prog*. 2006;106:25–57.
24. Green DW, Perry RH. *Perry's Chemical Engineers' Handbook*. New York, NY: McGraw-Hill, 2008.
25. Wilke CR. A viscosity equation for gas mixtures. *J Chem Phys*. 1950;18:517–519.
26. Yi JS, Nguyen TV. An along-the-channel model for proton exchange membrane fuel cells. *J Electrochem Soc*. 1998;145:1149–1159.
27. Moran PAP. Estimating structural and functional relationships. *J Multivar Anal*. 1971;1:232–255.
28. Patankar SV. *Numerical Heat Transfer And Fluid Flow*. New York, NY: Hemisphere Publishing Corporation, 1980.
29. Fiacco AV, McCormick GP. *Nonlinear Programming Sequential Unconstrained Minimization Techniques*. Philadelphia, PA: SIAM, 1990.
30. Fourer R, Gay DM, Kernighan BW. *AMPL: A Modeling Language for Mathematical Programming*. Belomont, CA: Duxbury Press, 1992.
31. Ticianelli EA, Derouin CR, Srinivasan S. Localization of platinum in low catalyst loading electrodes to attain high power densities in SPE fuel cell. *J Electroanal Chem*. 1988;251:275–295.
32. Suresh G, Pandey AK, Goswami A. Self-diffusion coefficients of water in Nafion-117 membrane with multivalent counterions. *J Memb Sci*. 2006;284:193–197.
33. Motupally S, Becker AJ, Weidner JW. Diffusion of water in Nafion 115 membranes. *J Electrochem Soc*. 2000;147:3171–3177.
34. Fuller TF, Newman J. Water and thermal management in solid-polymer-electrolyte fuel cells. *J Electrochem Soc*. 1993;140:1218–1225.
35. Larminie J, Dicks A. *Fuel Cell Systems Explained*. New York, NY: Wiley, 2002.
36. Schenk O, Wächter A, Hagemann M. Matching-based preprocessing algorithms to the solution of saddle-Point problems in large-scale nonconvex interior-point optimization. *Comput Optim Appl*. 2007;36:321–341.

Manuscript received Dec. 8, 2007, revision received Feb. 19, 2008, and final revision received Apr. 24, 2008.